

# Cardiac-evoked long-range quantum entanglement in the conscious brain

Christian M. Kerskens

*Institute of Neuroscience, Trinity College Dublin, Ireland*

David López Pérez

*Institute of Neuroscience, Trinity College Dublin, Ireland*

*Institute of Psychology, Polish Academy of Science, Warsaw, Poland*

We report observations of cardiac-evoked long-range zero quantum coherence (ceZQC) in human brain tissue which were not accompanied by an alternation of short-range quantum coherence. For every cardiac pulsation, ceZQC emerged over the entire brain tissue for a period of  $270 \pm 180$  ms. We observed this quantum effect in 40 human volunteers, if and only if they were awake. This link to conscious awareness suggests that the information held in the long-range quantum phenomenon is used and manipulated in conscious-related computation.

The MRI signal, which is single quantum coherence (SQC), is indirectly effected by short-range multiple quantum coherence (MQC) via  $T_1$  and  $T_2$  relaxation. Long-range MQC [1] may not effect the MRI signal significantly but it can be observed with the help of field modulation in so-called multiple spin echoes (MSEs) [2–4]. A basic MSE sequence consists of asymmetric magnetic field gradients, in contrast to the conventional single spin echo (SSE) methods where symmetry is essential, combined with at least two radio-frequency (RF) pulses [2–4]. For any "classical fluid", the signal-to-noise ratio in MSE, which depends on the probability of long-range multiple quantum coherence, is much lower than in SSE. For example, the signal ratio of ZQC to SQC only reaches up to 0.02 at 4 Tesla, experimentally [5, 6]. A SSE sequence could also contain MSEs if repeated fast. So-called crusher gradients (to dephase any SQC signal that remains from the previous excitation) which are added between two image acquisitions (see Fig. 1), produce an asymmetry in the subsequent acquisition [7]. In consecutive echo-planar imaging (EPI) time series, field modulations to create MSEs are accomplished in even numbered repetition. The asymmetric gradient field as shown in Fig. 1 can generate zero quantum orders [5] and higher negative orders [8]. Of course, fast imaging sequences have a high noise level (around 0.02) which means that ZQC signals are negligible in fast imaging series for any classical liquids. This is also the intention of the sequence design. However, we found, unexpectedly, ZQC signals in fast MR imaging which were evoked by the cardiac pulse. We studied 40 subjects [9] (between 18 and 46 years old) using a 3.0 Tesla whole-body MRI scanner [10]. In fast gradient-echo EPI (GE-EPI) time series [11], we found periods of predominant signal alternations repeated with the cardiac frequency (Fig. 2). In each cardiac cycle, we observed a period of around 4–6 TRs (180–270ms) (which varied between 2 TRs (90ms) and up to 10 TRs (450ms) under special circumstances) (Fig. 4B) where the averaged signal amplitude increased by up to 15 %. The evoked signal alternation confirmed

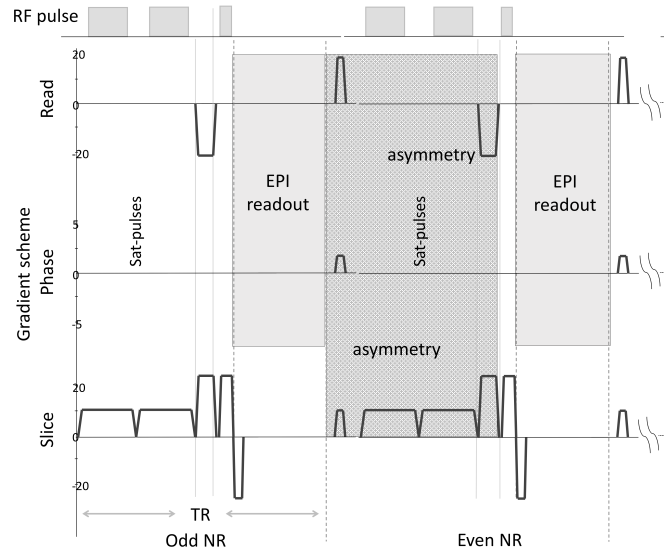


Abbildung 1. Radio frequency (RF) and Gradient scheme of two consecutive EPI acquisition. The "asymmetry" field includes all asymmetric gradients of the ZQC.

a ZQC contrast mechanism caused by the sequence design. It was also verified by altering the following sequence parameters; (a) rotation of the asymmetric gradients through slice rotation [12], (b) variation of the flip angle [13], and (c) alteration of the off-resonance frequency [14]. For the analysis, averaged maximum peak (AMP) and baseline signal (BS) [15] from pre-processed data [16] were calculated. For (a), we found the characteristic angulation dependency of the dipole-dipole interaction as shown in (Fig. 3(A)). The plot represents the fitted function  $|(3 \cdot \cos^2[\varphi] - 1)|$  (adjusted  $R^2$  test of goodness-of-fit resulted in  $R^2=0.9958$ ) where  $\varphi$  takes the additional gradients in read and phase direction into account which relates to the slice angulation as  $\varphi = \alpha - \tan^{-1} \left[ \frac{G_{t_{cru}} - G_{t_{rt}}}{2G_{t_{sat}} + G_{t_{cru}} + G_{t_{st}}} \right] = \alpha - 9.6^\circ$ . At the magic angle, the cardiac evoked signals disappeared

completely which rules out any SQC component. Consequently, we can exclude that the signal was generated by changes in  $T_1$  and  $T_2$  relaxation, line narrowing, or magnetic field shifts. It also means that short-range ZQC weren't significantly altered. For (b), we found the predicted signal course for the ZQC flip angle dependency [8] which was fitted to the data ( $R^2=0.9964$ ). Predicted maximum of AMP at  $45^\circ$  could be confirmed (Fig 3(B)). In contrast, the Ernst-angle [17] which is a good indication for the optimum angle for SQC is around  $13^\circ$  (for  $T_1 = 1.5$ s). For (c), we found a typical magnetization transfer contrast (MTC) change for the BS which depended on the off-resonance frequency (Fig. 3(C)). In contrast, the AMP intensity shows the remarkable immunity to MTC as expected for ZQC [18] with no significant changes in the same frequency range (Fig. 3(D)). Furthermore, the cardiac-evoked ZQC

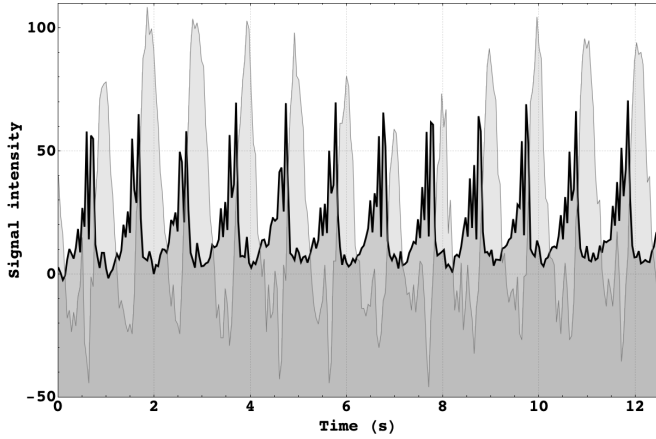


Figure 2. Whole-slice averaged signal time course (black line) which was selected by a mask over 12 heart cycles. Signal of the Superior sagittal sinus (grey line) as reference time frame demonstrates the instant breakdown of quantum coherence with the beginning outflow.

(ceZQC) also showed unseen physiological properties of which we observed the following here:

(1) Temporal occurrence – In our experiments, the ceZQC always appeared between the arterial inflow and the venous outflow phase. The finding was established with the help of reference time frames from (a) finger pulse oximetry (supplementary material (Fig. 4)), (b) from the MRI data itself by using a voxel including the superior sagittal sinus (Fig. 2) and (c) from a data set with a longer repetition time (TR) of 70 ms, which also allowed the simultaneous observation of arteries (supplementary material (Fig. 5)). All three methods confirmed a perfect synchronization with the cardiac pulse.

(2) Spatial distribution – Further, we explored the distribution of the ceZQC over the entire brain. 9 slices (in 5 volunteers) were acquired at different positions, with slices from bottom to the top covering all anatomical

regions. Test tubes with a water solution [19] were positioned close to the head for reference signals. We located ceZQC in brain tissue of all slices except around the periventricular area (probably due to movement induced by ventricular pulsation in those regions [20]) as shown in the supplementary material (Fig. 2). Regions like the skull and the attached test tubes showed no ceZQC excluding external signal sources. The sensitivity to movement could be confirmed in a hyperventilation challenge [21], where head movement was slightly altered. There, the signal declined immediately at the start of the challenge before any cerebral blood flow response could occur (supplementary material (Fig. 3)). The global aspect conformed with another interesting feature; the ceZQC signal could be restored while being averaged over the entire tissue component of the imaging slice (Figures 2 and 4(B)), which requires a traveling pulse that moves faster than the blood flow. (3) Blood

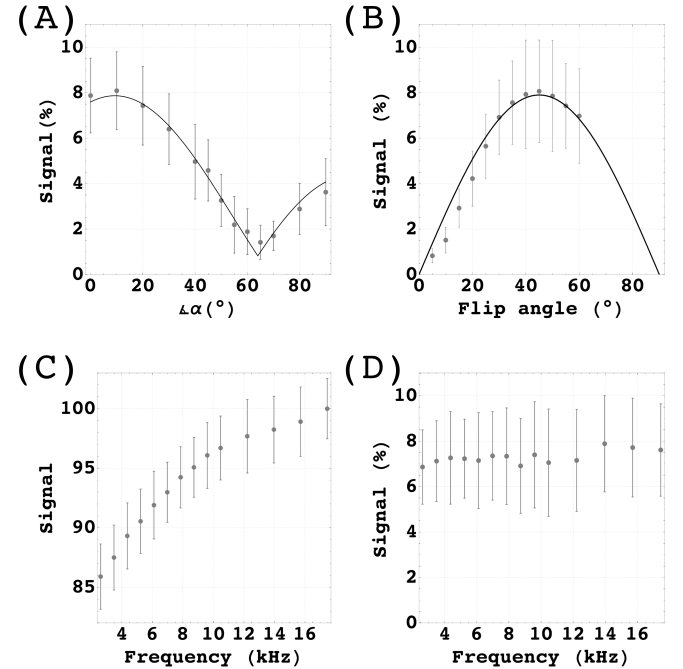


Figure 3. Variation of sequence parameters. Data shows signal averaged over 5 subjects. Error bars represent the standard deviation from the mean. (A) Signal intensity plotted against the slice gradient angulation  $\alpha$  in respect to the magnetic main field. (B) Signal plotted against flip angle variation. ZQC prediction plotted in Black. (C) Signal intensity plotted against the frequency offset of the saturation slices of the averaged baseline signal and (D) averaged signal of the zigzag.

flow relation – In a breath-holding challenge [22], we found that the ceZQC amplitude did not respond to the  $\text{CO}_2$  challenge (Fig. 4(B)), despite the fact, that we observed an increase of blood flow in major blood vessels during the challenge (Fig. 4(A)). Furthermore,

we found in a fMRI study [23], that local increase in blood perfusion during visual activation left the signal intensity undisturbed, too. We conclude from those observations that the signal intensity is not correlated to the cerebral blood flow directly. Further, we found that the AMP did not vary significantly with slice thickness [24] which confirmed the exclusion of movement and inflow as possible signal source (supplementary material (Fig. 6(A))). For the imaging repetition time (TR) [25], which defines the time-of-flight, no inflow effect could be detected either (supplementary material (Fig. 6(B))). (4) Conscious awareness – We found in

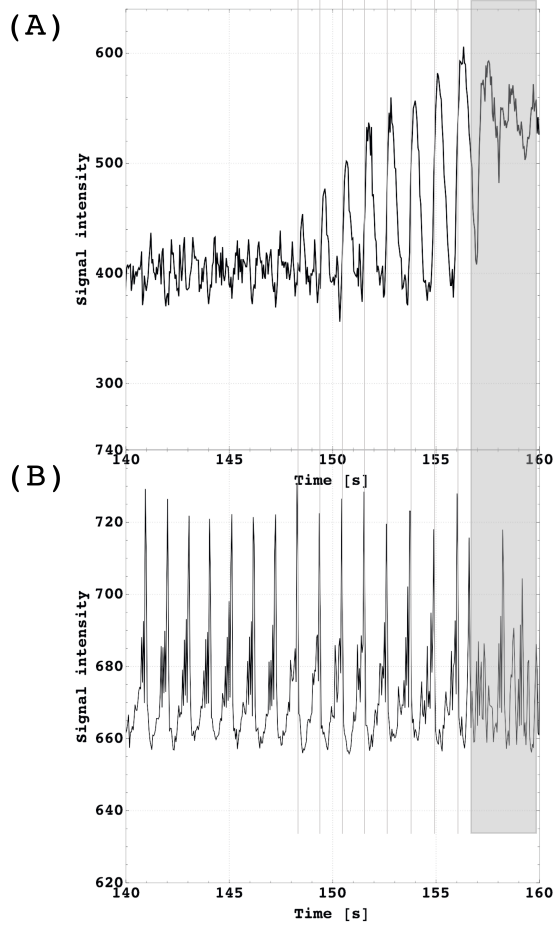


Figure 4. (A) Signal time course of an imaging voxel located next to the Superior sagittal sinus demonstrates the blood flow increase in response to the  $\text{CO}_2$  challenge (breath-holding). In contrast to the vein signal, the corresponding ceZQC signal (B) showed no response to  $\text{CO}_2$  activity. Breath-holding started at 140s. Volunteers were instructed to reduce any movement as long as possible (here until at 157s). From 157s, the signal breakdown was subject to movement.

seven participants from whom two had reported to have fallen asleep, that the ceZQC signal pattern changed dramatically as shown in Fig. 5. This dramatic signal pattern changed gradually during the transition from

awake to asleep as shown in the supplementary material (Fig. 7). In supplementary material at (Fig. 8), the results of a Recurrence Quantification Analysis and a Multifractal Detrended Fluctuation Analysis (for detailed description see Lopez-Perez et al. [26]) are plotted over all time points. The plots illustrate the difference between wakefulness and the slow decline during the falling asleep period. The analysis shows that periodicity, large and small fluctuations, repeating patterns and their predictability, and the stability of the system were changing over the observation period. In-depth analysis of sleep pattern and the effect of aging will be reported elsewhere [26]. For the final data acquisition, all participants had been asked to stay awake during the imaging protocol. Then, we no longer detected a sleep pattern. In conclusion, our

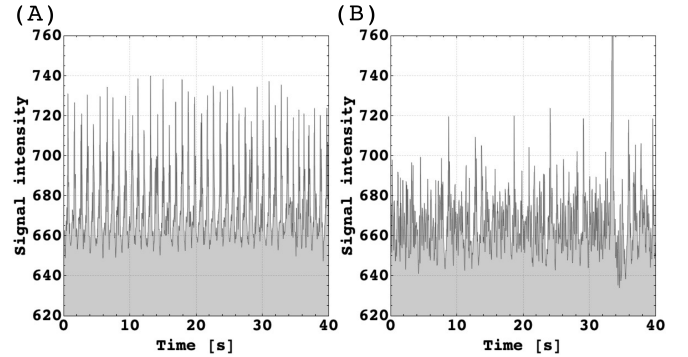


Figure 5. Pattern observed in participant who had reported falling asleep. (A) Wake period. (B) Asleep, ceZQC signal declined with an increase of signal noise level. At 34 s, the peak resulted from short head movement.

observation connects cardiac pulsation, which is a basic necessity for consciousness, with microscopic phenomena of the quantum world. A change of multiple quantum coherence, as observed here, is generally associated with a phase transition, which is consistent with our findings in a way that ceZQC was not caused by inflow or movement and further that it appeared and vanished in an instant and global fashion. However, a "classical" phase transition is always accompanied by a significant change of short-range multiple quantum coherence which was absent in our experiments. On the other hand, the existence of long-range (but without short-range) entanglement is the essence of topological order [27]. If we now consider that quantum coherence is equivalent to quantum entanglement for all practical purposes [28], then our observation suggests that we have found a topological-like phase in the conscious brain. Of course, it is not a topological phase as known from low temperature physics. However, active matter shows superfluid-like flow [29, 30]; similarly a topological-like phase may evolve in the brain featuring long-range

quantum entanglement. This topological-like phase could explain the link to conscious awareness; Taking into account that biological systems contain diversities of topological defects [31–34], which may also move in a céilidh dance fashion [35], then it is intriguing to assume that such defects are manipulating the information held in the topological-like order [36]. Such a process may provide a way to perform topological-like quantum computations which would imply that consciousness, and probably cognition also, is based on quantum computing.

D.L.P thanks Science Foundation Ireland for financial support (SFI-11/RFP.1/NES/3051).

- 
- [1] W. S. Warren, W. Richter, A. H. Andreotti, and B. T. Farmer, *Science* **262**, 2005 (1993).
- [2] G. Deville, M. Bernier, and J. M. Delrieux, *Physical Review B* (1979).
- [3] G. Eska, H. G. Willers, B. Amend, and C. Wiedemann, *Physica B+C* (1981).
- [4] R. Bowtell, R. M. Bowley, and P. Glover, *Journal of Magnetic Resonance* (1969) **88**, 643 (1990).
- [5] W. S. Warren, S. Ahn, M. Mescher, M. Garwood, K. Ugurbil, W. Richter, R. R. Rizi, J. Hopkins, and J. S. Leigh, *Science* **281**, 247 (1998).
- [6] R. R. Rizi, S. Ahn, D. C. Alsop, S. Garrett-Roe, M. Mescher, W. Richter, M. D. Schnall, J. S. Leigh, and W. S. Warren, *Magnetic Resonance in Medicine* **43**, 627 (2000).
- [7] Two saturation pulses placed parallel to the imaging slice (Fig. 1) are added which allow to vary the long-range correlation of the ZQC.
- [8] C. Zhong, Z. Shaokuan, and Z. Jianhui, *Chemical Physics Letters* **347**, 143 (2001).
- [9] Imaging protocols were approved by the Trinity College School of Medicine Research Ethics Committee. All participants of final data acquisition were asked to stay awake and stay still during the imaging protocol or to report any failure.
- [10] The scanner (Philips, The Netherlands) was operated with a 32-channel array receiver coil.
- [11] Initial experiments were carried out to establish a protocol that could deliver stable cardiac related signals over a range of subjects. The finalized parameters were as follows: FA = 45°, TR = 45 ms and the TE = 5 ms with a voxel size was 3.5 x 3.5 x 3.5 mm, matrix size was 64x64, SENSE factor 3, bandwidth readout direction was 2148 Hz, saturation pulse thickness/distance 5/20mm.
- [12] Slice angulation started from coronal 0° to axial 90° in the steps as [0, 10, 20, 30, 40, 45, 50, 55, 60, 65, 70, 80, 90]; Saturation gradients had a time integral (length x strength) of  $G_{t,sat} = 5.1 \text{ ms} \times 6.25 \text{ mT/m}$ , the crusher gradients in read and slice direction of  $G_{t,cru} = 1.3 \text{ ms} \times 25 \text{ mT/m}$ , the slice rephase gradient of  $G_{t,sr} = 0.65 \text{ ms} \times 25 \text{ mT/m}$ , the slice termination gradient of  $G_{t,st} = 0.65 \text{ ms} \times 15 \text{ mT/m}$ , and the total read dephase after EPI readout gradient of  $G_{t,rt} = 0.65 \text{ ms} \times 22.5 \text{ mT/m}$ .
- [13] The flip angle was varied from 5° to 60° in steps of 5°(60° was the power limit by the specific absorption rate (SAR)).
- [14] The off-resonance frequencies was varied as [2.62, 3.49, 4.36, 5.23, 6.11, 6.98, 7.84, 8.73, 9.60, 10.47, 12.22, 13.96, 15.71, 17.45] kHz.
- [15] E. F. Gomes, A. M. Jorge, and P. J. Azevedo, in *Proceedings of the International C\* Conference on Computer Science and Software Engineering* (ACM, 2013) pp. 23–30.
- [16] Data were processed with Matlab 2014a (<http://www.mathworks.co.uk/>). Rescaling was applied to all data sets before any analysis using the MR vendor's instructions. Average time series were visually inspected in search for irregularities which were manually removed from the analysis leaving the rest of the time series unaltered. Manual segmentation was used to create a mask to remove cerebral spinal fluid (CSF) contributions. The first 100 of 1000 scans were removed to avoid signal saturation effects. The manual segmentation of the masks was eroded to avoid partial volume effects at the edges. For the analysis, we made use of the fact that the signal is highly coherent over the entire slice (for more details see below (2)).
- [17] R. R. Ernst and W. A. Anderson, *Review of Scientific Instruments* **37**, 93 (1966).
- [18] E. Uzi and N. Gil, *Journal of Magnetic Resonance* **190**, 149 (2008).
- [19] Solution composition: 1000 ml demineralized water contained 770 mg CuSO<sub>4</sub>·5H<sub>2</sub>O, 1 ml Arquad (AkzoNobel), 0.15 ml H<sub>2</sub>SO<sub>4</sub>-(0.1 N)).
- [20] R. Nunes, P. Jezzard, and S. Clare, *J Magn Reson* **177**, 102 (2005).
- [21] During indicated intervals four participants were asked to hyperventilate for 40 s with three repeats.
- [22] During indicated intervals the subjects were asked to stop breathing for 20 s with out taken a deep breath. Body movements were reduced through multiple cushions immobilizing the head.
- [23] D. López-Pérez, *Non-Single Quantum MRI: A Cardiac Modulated Rhythm in the Brain Tissue*, Ph.D. thesis, Medicine, Trinity College Dublin (2016).
- [24] Slice thickness from 3 mm to 7 mm in steps of 0.5 mm.
- [25] TR varied from 38 ms to 73 ms in steps of 5 ms.
- [26] Lopez-Perez, “Complexity Changes of the Long-range Spin-spin Interactions in the Human Brain.”
- [27] X. Chen, Z.-C. Gu, and X.-G. Wen, *Physical Review B* **82** (2010), 10.1103/physrevb.82.155138.
- [28] A. Streltsov, U. Singh, H. S. Dhar, M. N. Bera, and G. Adesso, *Physical Review Letters* **115** (2015), 10.1103/physrevlett.115.020403.
- [29] M. E. Cates, S. M. Fielding, D. Marenduzzo, E. Orlandini, and J. M. Yeomans, *Physical Review Letters* **101** (2008), 10.1103/physrevlett.101.068102.
- [30] H. M. López, J. Gachelin, C. Douarche, H. Auradou, and E. Clément, *Physical Review Letters* **115** (2015), 10.1103/physrevlett.115.028301.
- [31] N. Kumar, R. Zhang, J. J. de Pablo, and M. L. Gardel, *Science Advances* **4**, eaat7779 (2018).
- [32] G. Duclos, C. Erlenkämper, J.-F. Joanny, and P. Silberzan, *Nature Physics* **13**, 58 (2016).
- [33] K. Kawaguchi, R. Kageyama, and M. Sano, *Nature* **545**, 327 (2017).
- [34] T. B. Saw, A. Doostmohammadi, V. Nier, L. Kocgozlu, S. Thampi, Y. Toyama, P. Marcq, C. T. Lim, J. M. Yeomans, and B. Ladoux, *Nature* **544**, 212 (2017).

- [35] A. Doostmohammadi, J. Ignés-Mullol, J. M. Yeomans, and F. Sagués, *Nature Communications* **9** (2018), 10.1038/s41467-018-05666-8.
- [36] M. H. Freedman, A. Kitaev, M. J. Larsen, and Z. Wang, *Bulletin of the American Mathematical Society* **40**, 31 (2002).